Elastic-scattering effects on resonant tunneling in double-barrier quantum-well structures

H. A. Fertig, Song He, and S. Das Sarma
Center for Theoretical Physics and Department of Physics and Astronomy, University of Maryland, College Park, Maryland 20742-4111
(Received 1 September 1989)

We investigate, using a microscopic perturbation theory, the effects of elastic scattering on resonant tunneling in double-barrier quantum-well structures. Using a perturbation expansion in the scattering strength, we calculate corrections to the average transmission matrix for low impurity densities. For two- and three-dimensional structures in the absence of a magnetic field, the Lorentzian line shape associated with tunneling events that conserve transverse momentum is broadened asymmetrically by impurity scattering. There are also contributions to the tunneling probability that do not conserve transverse momentum; for incident energy $\varepsilon > E_0$, where E_0 is the resonant energy, this contribution is strongly peaked when the energy of motion perpendicular to the well closely matches E_0. This leads to a "focusing" of electrons into a particular set of final states. In the absence of a magnetic field, a striking spatial distribution in the tunneling probability results. For the total tunneling current, our microscopic theory gives results consistent with a Breit-Wigner-type formula for the impurity scattering induced broadening. For the case in which a magnetic field is applied perpendicular to the well region, we find that the "focused" electrons tend to scatter into Landau levels n such that $\varepsilon-(n+\frac{1}{2})\omega_0$ is as close as possible to E_0. We also find a broadening of the usual Lorentzian contribution to the tunneling probability in the magnetic field case and an upward shift in the resonant energy that varies logarithmically with magnetic field. Finally, we test our predictions numerically by calculating the exact transmission matrix for a finite two-dimensional system; the results are in good qualitative agreement with the perturbation theory analysis. Our numerical work also shows that for stronger disorder scattering, the conductance is a direct measure of the density of states inside the well.

I. INTRODUCTION

In recent years, there has been a great deal of interest in resonant tunneling through double-barrier quantum-well (DBQW) devices. Such structures exhibit negative differential resistance, making them promising candidates for device applications.[1] With the improved quality of samples available in the recent past,[2] there has been an ever increasing demand for a detailed understanding of their I-V characteristics. Qualitatively, the behavior of these structures has been understood for some time.[3] However, most studies of important perturbations such as electron-phonon and electron-impurity interactions have been phenomological in nature[4,5] and, furthermore, are explicitly calculations for one-dimensional systems. This latter limitation makes detailed comparison with experiment difficult even on a qualitative level. Recently, a number of workers have considered microscopic models that address in detail the effects of electron-phonon[6,7] and electron-electron[8] interactions. These studies are also, for the most part, limited to one-dimensional models.[6,8]

In this work, we will study two- and three-dimensional microscopic models for the purpose of understanding the effect of elastic scattering in the DBQW system. Some of these results have been briefly reported elsewhere;[9] in this article, we will give details of our calculations as well as the results of exact numerical calculations that support our perturbative approach. We consider a model in which a well region is weakly coupled to reservoirs on the right and left. (Similar models have been used to study resonant tunneling in one-dimensional systems.[6,8]) The weak links represent the barrier regions of the DBQW system, and in the absence of coupling to the reservoirs, the energy spectrum for electrons in the well is taken to have the form $E_0+\varepsilon_\alpha^{\parallel}$. Here, E_0 is the resonant energy, and $\varepsilon_\alpha^{\parallel}$ represents the energy of motion parallel to the well region. We consider both two- and three-dimensional samples in the absence of a magnetic field, and a three-dimensional sample with a magnetic field applied perpendicular to the well region. Impurities in our models are confined to the well region. In all cases, we will be evaluating the transmission matrix $T(\alpha,\beta;\varepsilon)$, which is a generalization of the transmission coefficient often studied in one-dimensional scattering problems. Here, α and β represent quantum numbers associated with motion parallel to the well region. In the absence of a magnetic field, they are just momenta, (i.e., $\alpha=\mathbf{p}_{\text{in}}$, $\beta=\mathbf{p}_{\text{out}}$); in the presence of a magnetic field, they include both a Landau-level index and a one-dimensional momentum. The transmission matrix should be understood as the probability that an electron with energy ε initially on the left of the well region in state α tunnels through the DBQW structure into a state β on the right.

In Sec. III of this work, we calculate, using perturbation theory, the effect of a small density of impurities in the well on the average transmission matrix $\langle T(\alpha,\beta;\varepsilon)\rangle$. We find that $\langle T\rangle$ is most conveniently expressed as a sum of terms, each of which enters at a specified order in

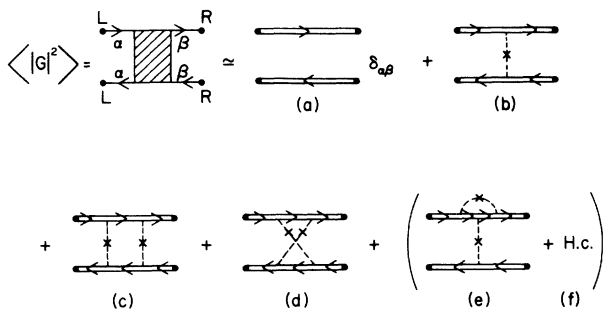

FIG. 1. Diagrammatic expansion of $\langle T \rangle$ to second order in the impurity density.

the impurity density, and all of which are specified by diagrams such as those shown in Fig. 1. Specifically, Fig. 1(a) is proportional to $T^{(0)}$, Fig. 1(b) to $T^{(1)}$, and the sum of Figs. 1(c)–1(f) will specify $T^{(2)}$. $T^{(i)}$ is thus the ith-order contribution to the transmission matrix. We begin by discussing our results for a sample in the absence of a magnetic field. The lowest-order contribution, $T^{(0)}$, is overwhelmingly the largest contribution to the tunneling probability in the weak-scattering limit. We note that $T^{(0)}$ contains only processes that conserve momentum parallel to the well region. As a function of ε, $T^{(0)}(\alpha,\beta;\varepsilon)$ turns out to have essentially the usual Lorentzian behavior associated with resonant tunneling;[3] however, there is an increased linewidth and a small asymmetry introduced by the self-energy correction due to impurity scattering.

More interesting than this are processes that allow the transverse momentum to change. With $\mathbf{p}_{\text{in}} \equiv \alpha$ and $\mathbf{p}_{\text{out}} \equiv \beta$, the lowest-order contribution that allows this is $T^{(1)}(\mathbf{p}_{\text{in}}, \mathbf{p}_{\text{out}};\varepsilon)$, Fig. 1(b). We will find that $T^{(1)}$ is easily evaluated and that it has a number of interesting properties. Most importantly, we find that for fixed $\mathbf{p}_{\text{in}}$ and ε, $T^{(1)}$ is strongly peaked when $\varepsilon - p_{\text{out}}^2/(2m) = E_0$. This leads to a pronounced spatial distribution that may be described as a focusing effect, since certain momentum states $\mathbf{p}_{\text{out}}$ are picked out as favored final states.

To illustrate the focusing effect more clearly, it is convenient to study a two-dimensional DBQW system. In Fig. 2, we display as a function of p_{out} the behavior of $T^{(1)}(p_{\text{in}},p_{\text{out}};\varepsilon)$ for $p_{\text{in}}=0$ and two values of ε. For the case $\varepsilon < E_0$, the electron "sprays" out into an angular distribution of about 1 rad. For the case $\varepsilon > E_0$, one finds two sharp peaks located at $\pm\theta_0$ satisfying $\varepsilon - p^2/(2m) = \varepsilon \cos^2\theta_0 = E_0$. This unique double peaking is a direct result of the combination of elastic scattering and resonant tunneling.

The two-dimensional system is of further interest because one can evaluate all the contributions to $T^{(2)}(p_{\text{in}},p_{\text{out}};\varepsilon)$ [Figs. 1(c)–1(f)] to see how higher-order terms contribute to the transmission matrix. In Fig. 3, we illustrate a typical example of $T^{(2)}$ for $\varepsilon > E_0$; the electron is taken to be incident from the second quadrant in the inset of Fig. 2. The basic double-peak structure is the same as that of $T^{(1)}$. However, we see the $\theta_0 > 0$ peak is larger than the $\theta_0 < 0$ peak. This behavior is related to weak localization, as will be explained in Sec. III.

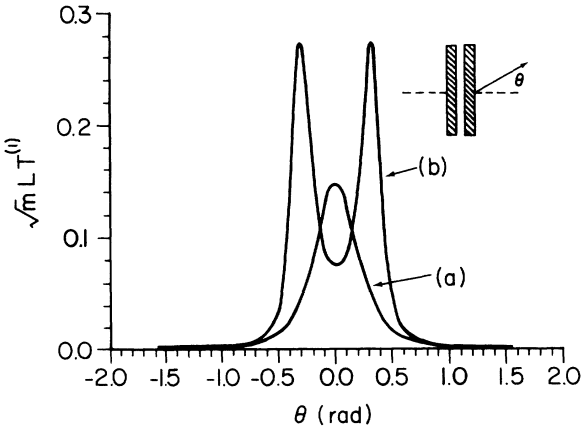

FIG. 2. First-order correction to transmission matrix $T^{(1)}(p_{\text{in}},p_{\text{out}};\varepsilon)$ as a function of exit angle θ, for a two-dimensional system, with $p_{\text{in}}=0$. Energy scale is set by $E_0=1$, and we take $\Gamma_0=0.1$. Disorder parameter $\alpha_2=0.2$, and (a) $\varepsilon=0.9$ and (b) $\varepsilon=1.1$. Inset: geometry specifying $\theta=\arctan(p_{\text{out}}/k_z)$, where $k_z=(2m\varepsilon-p_{\text{out}}^2)^{1/2}$.

We have also examined a three-dimensional DBQW model in which a magnetic field is applied perpendicular to the well region. In this case, working in the Landau gauge, the electron states are characterized by transverse quantum numbers n and p, where n is a Landau-level index and p is a one-dimensional momentum. The analysis in this case is considerably more complicated than in the absence of a magnetic field, and so we restrict our calculations to lowest nontrivial order in the impurity density. As in the nonmagnetic field case, the lowest-order contribution to the transmission matrix conserves the transverse quantum numbers [i.e., $T^{(0)}(\alpha,\beta;\varepsilon) \propto \delta_{\alpha\beta}$]. As a function of ε, $T^{(0)}$ is nearly Lorentzian, with a small broadening due to the self-energy correction. We also find that the real part of the self-energy introduces a

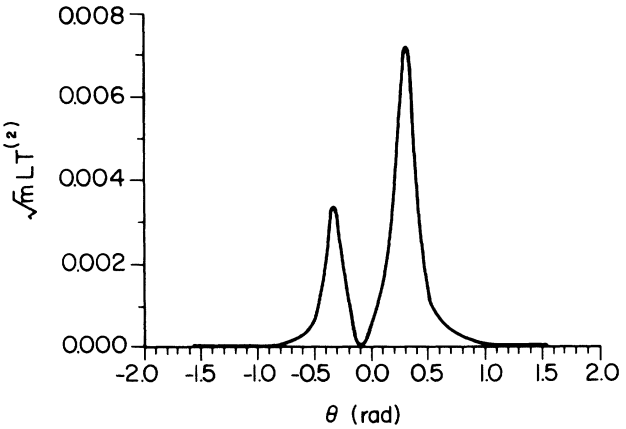

FIG. 3. Second-order correction to transmission matrix $T^{(2)}(p_{\text{in}},p_{\text{out}};\varepsilon)$ as a function of θ. $E_0=1$, $\Gamma_0=0.1$, $\alpha_2=0.2$, $\varepsilon=1.1$, and $\varepsilon^{\parallel}_{p_{\text{in}}}=0.5$. Exit angle θ is defined as in Fig. 2.

small increase in the resonant energy that varies logarithmically with magnetic field.

In addition to $T^{(0)}$, there are also processes contributing to the average transmission matrix which do not conserve the transverse quantum numbers. To the lowest nontrivial order, these are described by Fig. 1(b), and as usual are denoted by $T^{(1)}(\alpha,\beta;\varepsilon)$. We find that $T^{(1)}$ is only significant if the final momentum p_β is within a few magnetic lengths of the initial momentum, p_α. It is useful to sum over final momentum states and consider the distribution of final Landau indices for the tunneling electron. For fixed incident Landau index n_α and energy ε, we find that $T^{(1)}$ is maximized when $\varepsilon-(n_\beta+\frac{1}{2})\omega_c$ is as close as possible to E_0, where $\omega_c=eB/mc$ is the cyclotron frequency. This is the analog of the focusing effect we found for the nonmagnetic field case.

To check the validity of the perturbation theory analysis, we have evaluated numerically the exact transmission matrix for a two-dimensional tight-binding model. We find good qualitative agreement between the perturbation-theory results and the exact results for a finite system if we average over several impurity realizations. The largest contribution to the tunneling probability comes from the conserved momentum channel; at a much smaller amplitude, one finds transmission into other momentum states, with a distribution that has a double-peak structure very similar to that shown in Fig. 2. Furthermore, one can discern that the backscattering peak indeed has slightly more weight than the "forward"-scattering peak, as we found in the perturbation-theory analysis. We remind the reader that in this context, forward scattering and backscattering refer only to the directions of the two peaks relative to the incident momentum, and are *not* specified by $p_{\rm out}=\pm p_{\rm in}$.

The main difference between our perturbation theory results and the exact finite-size results is that the finite-size system has fluctuations superimposed on the double-peak structure. These fluctuations smooth out as one averages over a large number of impurity realizations. For a single realization, the fluctuations are quite strong, and the transmission matrix T may drop to zero many times as a function of the exit angle θ. However, these fluctuations are contained within an envelope function that has the double-peak structure expected for the average transmission matrix. Thus, we find empirically that a form of the focusing effect should be expected even in a single sample at $T=0$, for which the impurity-averaging procedure used in the perturbation-theory analysis is not expected to be valid.

We have also investigated the total current for both large and small bias. In two dimensions, and for small disorder, we find good qualitative agreement between the perturbation-theory analysis and the numerical results. For larger disorder, we find empirically that the differential current—which is essentially the conductance of the system—can be used to directly probe the density of states inside the well.

This paper is organized as follows. In Sec. II, we describe in some detail the models used for our DBQW structures and the impurity potentials inside the well. In Sec. III A, we outline the general procedure for calculating the average transmission matrix in perturbation theory. The remainder of Sec. III describes our results for the models we study. In Sec. IV, we discuss our numerical results for the finite-two-dimensional system, and we conclude with a summary in Sec. V.

II. THE MODELS

In this work, we will consider two distinct models for a DBQW system with impurities in the well. The first is a natural generalization to three dimensions of a one-dimensional resonant-tunneling model studied by other workers.[6,8] We consider a tight-binding Hamiltonian in d dimensions, where all the on-site energies are the same, except on a $(d-1)$-dimensional plane that models the well region. The amplitude of the hopping terms connecting this plane to the left and right reservoirs are purposely chosen to be small, to model the barrier regions of the DBQW structure. In the site representation, the Hamiltonian takes the form

$$H=t^L\sum_{\langle n,m\rangle}(a^\dagger_{L,n}a_{L,m}+\text{H.c.})+t^R\sum_{\langle n,m\rangle}(a^\dagger_{R,n}a_{R,m}+\text{H.c.})+V^L\sum_{\langle n,m\rangle}(b^\dagger_n a_{L,m}+\text{H.c.})$$

$$+V^R\sum_{\langle n,m\rangle}(b^\dagger_n a_{R,m}+\text{H.c.})+\sum_n\varepsilon_n b^\dagger_n b_n+t_w\sum_{\langle n,m\rangle}(b^\dagger_n b_m+\text{H.c.})\,,$$

where the sums $\langle n,m\rangle$ are over nearest neighbors, $a^\dagger_{L,m}$ creates an electron at the mth site on the left, $a^\dagger_{R,m}$ creates an electron on the right, and $b^\dagger_n$ creates an electron in the well region. For calculational purposes, it is more convenient to work in a momentum representation, for which the Hamiltonian is

$$H=\sum_{k_z,\mathbf{p}}(\varepsilon_{k_z}+\varepsilon^{\parallel}_{\mathbf{p}})(c^\dagger_{L,k_z\mathbf{p}}c_{L,k_z\mathbf{p}}+c^\dagger_{R,k_z\mathbf{p}}c_{R,k_z\mathbf{p}})+V^L\sum_{k_z,\mathbf{p}}(c^\dagger_{L,k_z\mathbf{p}}d_{\mathbf{p}}+d^\dagger_{\mathbf{p}}c_{L,k_z\mathbf{p}})$$

$$+V^R\sum_{k_z,\mathbf{p}}(c^\dagger_{R,k_z\mathbf{p}}d_{\mathbf{p}}+d^\dagger_{\mathbf{p}}c_{R,k_z\mathbf{p}})+\sum_{\mathbf{p}_1,\mathbf{p}_2}E_{\mathbf{p}_1,\mathbf{p}_2}d^\dagger_{\mathbf{p}_1}d_{\mathbf{p}_2}\,, \tag{2.1}$$

where

$$c_{L(R),k_z\mathbf{p}} \equiv \frac{1}{\sqrt{N}} \sum_n e^{ik_z(\mathbf{R}_n\cdot\hat{\mathbf{z}})+i\mathbf{p}\cdot\mathbf{R}_n} a_{L(R),n} ,$$

N is the number of sites in a reservoir, $\mathbf{R}_n$ is the position of the nth site, $\mathbf{p}$ is a $(d-1)$-dimensional vector that lies in the $\hat{\mathbf{x}}$-$\hat{\mathbf{y}}$ plane, and the $\hat{\mathbf{z}}$ direction is perpendicular to the well region. The energies ε_{k_z} and $\varepsilon_p^{\parallel}$ are approximated by $k_z^2/2m$ and $p^2/2m$, respectively. The operators $d_{\mathbf{p}}$ are given by

$$d_{\mathbf{p}} = \frac{1}{\sqrt{M}} \sum_m e^{i\mathbf{p}\cdot\mathbf{R}_m^W} b_m ,$$

where $\mathbf{R}_m^W$ is the mth site inside the well region, and M is the number of sites within the well. The matrix elements $E_{\mathbf{p}_1\mathbf{p}_2}$ are given by

$$E_{\mathbf{p}_1\mathbf{p}_2} = \frac{1}{M} \sum_m e^{i(\mathbf{p}_2-\mathbf{p}_1)\cdot\mathbf{R}_m^W} \varepsilon_m .$$

To model a weak random potential, we take $\varepsilon_m = E_0 + \delta\varepsilon_m$, where $\delta\varepsilon_m$ is a random variable satisfying $\overline{\delta\varepsilon_m} = 0$ and $\overline{\delta\varepsilon_m \delta\varepsilon_n} = \mu\delta_{mn}$. The bars represent averages over the random variables, and the covariance μ will be small in the models we consider. We then have

$$E_{\mathbf{p}_1\mathbf{p}_2} = (E_0 + \varepsilon_{p_1}^{\parallel})\delta_{\mathbf{p}_1,\mathbf{p}_2} + U_{\mathbf{p}_1\mathbf{p}_2}$$

with

$$\overline{U^*_{\mathbf{p}_1\mathbf{p}_2} U_{\mathbf{p}_3\mathbf{p}_4}} = \frac{\mu}{M}\delta_{\mathbf{p}_1+\mathbf{p}_4,\mathbf{p}_2+\mathbf{p}_3} .$$

Higher-order variances (e.g., $\overline{U_1U_2U_3U_4}$) are taken to be equal to all possible combinations of averages of pairs (e.g., $\overline{U_1U_2}\,\overline{U_3U_4}$), which is a standard property of Gaussian randomness. A simple way to understand this model is to imagine that each lattice site in the well has some probability p of being occupied by an impurity. An occupied site has excess energy $\delta\varepsilon_n = (1-p)V_0$, and an unoccupied site $\delta\varepsilon_n = -pV_0$. (Strictly speaking, the higher-order variances in this model have a Gaussian form only in the limit $M\to\infty$.) For $p \ll 1$, one finds $\mu \simeq pV_0^2$, and p may be taken to be $p = \rho_{\text{imp}} a^{(d-1)}$, where ρ_{imp} is the areal density of impurities in the well, and $a^{(d-1)}$ is the area of a lattice site, which for consistency should be taken as the size of an impurity. We thus see that an expansion in μ is equivalent to an expansion in the impurity density.

The second model we consider is one in which a magnetic field is applied perpendicular to the well region. In this case, it is convenient to start with a Hamiltonian of the form in Eq. (2.1), specifically,

$$H = \sum_{k_z,n,p} (\varepsilon_{k_z} + \varepsilon_n^{\parallel})(c^{\dagger}_{L,k_znp} c_{L,k_znp} + c^{\dagger}_{R,k_znp} c_{R,k_znp}) + \sum_{n,p} (E_0 + \varepsilon_n^{\parallel}) d^{\dagger}_{np} d_{np} + c^{\dagger}_{R,k_znp} cR, k_z np)$$
$$+ \sum_{n_1,n_2} \sum_{p_1,p_2} U_{n_1n_2}(p_1,p_2) d^{\dagger}_{n_1p_1} d_{n_2p_2} + V^L \sum_{k_z,n,p} (c^{\dagger}_{L,k_znp} d_{np} + \text{H.c.}) + V^R \sum_{k_z,n,p} (c^{\dagger}_{R,k_znp} d_{np} + \text{H.c.}) . \quad (2.2)$$

The indices n are Landau indices, and $c^{\dagger}_{L(R)k_znp}$ creates an electron in the left (right) reservoir with wave function

$$\phi_{k_znp}(\mathbf{r}) = \frac{1}{\sqrt{L}} e^{ik_z z} \chi_{np}(x,y) ,$$

where

$$\chi_{np}(x,y) = \left[\frac{1}{\sqrt{\pi} l_0 L 2^n n!}\right]^{1/2} e^{ipy-(x+pl_0^2)^2/2l_0^2} \times H_n((x+pl_0^2)/l_0) ,$$

where L is the linear dimension of the reservoir, $l_0 = (\hbar c/eB)^{1/2}$ is the magnetic length, and H_n is the nth Hermite polynomial. Similarly, $d^{\dagger}_{np}$ creates an electron in the well with wave function $f(z)\chi_{np}(x,y)$; for simplicity, we taken $|f(z)|^2 = \delta(z)$. The energies ε_{k_z} and $\varepsilon_n^{\parallel}$ are, respectively, $k_z^2/2m$ and $(n+\frac{1}{2})\omega_c$, where $\omega_c = eB/mc$ is the cyclotron frequency.

The $U_{n_1n_2}(p_1,p_2)$ term is due to an interaction with a short-ranged, white-noise potential inside the well. In this case, we fix the number of impurities, and impurity averages are taken by integrating over their positions.[10] For a given impurity realization, one finds

$$U_{n_1n_2}(p_1,p_2) = a^2V_0 \left[\frac{1}{\pi l_0^2 L^2 n_1! n_2! 2^{n_1+n_2}}\right]^{1/2} \sum_i e^{i(p_2-p_1)y_i - [(x_i+p_1l_0^2)^2+(x_i+p_2l_0^2)^2]/2l_0^2} \times H_{n_1}((x_i+p_1l_0^2)/l_0) H_{n_2}((x_i+p_2l_0^2)/l_0) ,$$

where $\mathbf{r}_i = (x_i, y_i, 0)$ is the ith impurity position, and the potential due to this impurity is given by $a^2V_0\delta(x-x_i)\delta(y-y_i)$. The impurity averages in this model are considerably more difficult than in the tight-binding model. For this reason, we confine ourselves to lowest nontrivial order in perturbation theory in the magnetic field model.

III. PERTURBATION THEORY

A. General formulation

In this section, we outline the technique by which one calculates the average transmission matrix $\langle T(\alpha,\beta;\varepsilon)\rangle$. Here, α and β are quantum numbers that represent

momentum vectors in the absence of a magnetic field, and Landau indices and one-dimensional momenta in the presence of a magnetic field. The diagrammatic method used here is very similar to that used in the study of the x-ray singularity problem in photoemission.[11] The transmission matrix is defined as

$$T(\alpha,\beta;\varepsilon)=\int dk_z\,\delta(k_z-[2m(\varepsilon-\varepsilon_\alpha^{\parallel})]^{1/2}) \times\sum_{k_z'}\Gamma(k_z\alpha;k_z'\beta)/I(k_z,\alpha)\ , \tag{3.1}$$

where $I(k_z,\alpha)$ is the current incident upon the well region for an electron in the state (k_z,α), and $\Gamma(k_z\alpha;k_z'\beta)$ is the transition rate for an electron initially in state (k_z,α) in the left reservoir to tunnel into a state (k_z',β) in the right reservoir. The transmission matrix $T(\alpha,\beta;\varepsilon)$ represents a generalization of the transmission coefficient often studied in one-dimensional scattering problems. Using formal scattering theory,[12,13] the transition rate Γ may be expressed in terms of the T matrix:

$$\Gamma(k_z\alpha;k_z'\beta)=|\langle k_z'\beta|UGU|k_z\alpha\rangle|^2\ , \tag{3.2}$$

where

$$U=V^L\sum_{k_z,\alpha}(c^\dagger_{L,k_z\alpha}d_\alpha+\text{H.c.}) +V^R\sum_{k_z,\alpha}(c^\dagger_{R,k_z\alpha}d_\alpha+\text{H.c.})\ , \tag{3.3}$$

and

$$G(\varepsilon)=\frac{1}{\varepsilon-H+i\delta}\ .$$

Substitution of (3.3) into (3.2) gives

$$\Gamma(k_z\alpha,k_z'\beta)=|V^L|^2\,|V^R|^2\,|\langle 0|d_\beta G d^\dagger_\alpha|0\rangle|^2\ . \tag{3.4}$$

The matrix element here is a vacuum expectation value, which is appropriate when considering a single-particle tunneling event. Defining the partial widths[6] $\Gamma_0^{L,R}(\varepsilon)=2\pi\sum_{k_z}|V^{L,R}|^2\,\delta(\varepsilon-\varepsilon_{k_z})$, the average transmission matrix takes the form

$$\langle T(\alpha,\beta;\varepsilon)\rangle=\Gamma_0^L(\varepsilon-\varepsilon_\alpha^{\parallel})\Gamma_0^R(\varepsilon-\varepsilon_\beta^{\parallel})\langle|G_{\alpha\beta}(\varepsilon)|^2\rangle\ , \tag{3.5}$$

where we have adopted the notation $G_{\alpha\beta}(\varepsilon)\equiv\langle 0|d_\beta G d^\dagger_\alpha|0\rangle$, and the angular brackets here denote an impurity average. Thus, we have reduced the problem of finding the transmission matrix to the calculation of a Green's function.

In the absence of impurity scattering, the Hamiltonian conserves the transverse quantum numbers α, so that $G_{\alpha\beta}(\varepsilon)\propto\delta_{\alpha\beta}$. In this situation, the evaluation of the Green's function reduces to a one-dimensional problem for each α, for which there is a well-known exact solution. Following Mahan,[11] one finds

$$G^0_\alpha(\varepsilon)\equiv G_{\alpha\alpha}(\varepsilon)=\frac{1}{\varepsilon-\varepsilon_\alpha^{\parallel}-E_0-\Sigma^0_\alpha(\varepsilon)+i\delta}\ , \tag{3.6}$$

where

$$\Sigma^0_\alpha(\varepsilon)=(|V^L|^2+|V^R|^2)\sum_{k_z}\frac{1}{\varepsilon-\varepsilon_\alpha^{\parallel}-\varepsilon_{k_z}+i\delta}\ .$$

The imaginary part of the self-energy is given by

$$\text{Im}\Sigma^0_\alpha(\varepsilon)=-\pi(|V^L|^2+|V^R|^2)\sum_{k_z}\delta(\varepsilon-\varepsilon_\alpha^{\parallel}-\varepsilon_{k_z}) \equiv-\tfrac{1}{2}[\Gamma_0^L(\varepsilon-\varepsilon_\alpha^{\parallel})+\Gamma_0^R(\varepsilon-\varepsilon_\alpha^{\parallel})]\ .$$

This connection between the imaginary part of the self-energy and the partial widths was first noted in a different context by Langreth.[13] The transmission matrix for pure system may be written as

$$T^{\text{pure}}(\alpha,\beta;\varepsilon)=\frac{\Gamma_0^L(\varepsilon-\varepsilon_\alpha^{\parallel})\Gamma_0^R(\varepsilon-\varepsilon_\alpha^{\parallel})\delta_{\alpha\beta}}{[\varepsilon-\varepsilon_\alpha^{\parallel}-E_0-\text{Re}\Sigma^0(\varepsilon-\varepsilon_\alpha^{\parallel})]^2+[\Gamma_0(\varepsilon-\varepsilon_\alpha^{\parallel})/2]^2}\ , \tag{3.7}$$

where $\Gamma_0\equiv\Gamma_0^L+\Gamma_0^R$. Ignoring the energy dependence of the self-energy, we arrive at the Lorentzian "Breit-Wigner" behavior for the transmission coefficient that is expected for resonant-tunneling systems.[3,12] In all of what follows, we will adopt the approximation that Σ^0 is energy independent ($\text{Re}\Sigma^0$ is then absorbed into a redefinition of E_0 and will not be referred to explicitly again). For a one-dimensional system, the approximation that Γ_0^L and Γ_0^R are constants is equivalent to assuming that the density of states in the reservoirs is constant. More generally, our approximation will be valid so long as $\Sigma^0(\varepsilon)$ varies slowly in the vicinity of the resonance; i.e.,

$$\left.\frac{d\Sigma^0(\varepsilon)}{d\varepsilon}\right|_{\varepsilon=E_0}\ll 1\ .$$

The effect of a small impurity-scattering term in the Hamiltonian may be treated perturbatively. To calculate $\langle|G_{\alpha\beta}|^2\rangle$, we need to evaluate a vertex function, as shown in Fig. 1, with some of the lowest-order diagrams in the perturbation expansion. The dashed lines with crosses represent averaged impurity interactions. For the tight-binding model, the value assigned to an impurity line is just μ/m; in the magnetic field model, its value is considerably more complicated and in general can be evaluated only for specific choices of the Landau-level indices entering and leaving the impurity lines. We note

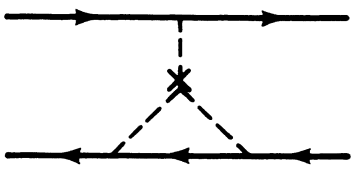

FIG. 4. Higher-order diagram not included in the diagrammatic analysis of the magnetic field model.

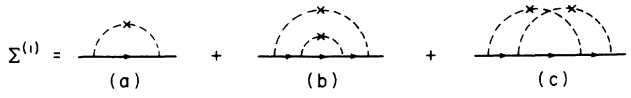

FIG. 5. Diagrammatic expansion of the self-energy.

also that diagrams like those shown in Fig. 4 should be evaluated for the magnetic field model; however, we will restrict ourselves to lowest order in the impurity density for this case and hence, will not consider such contributions.

The double lines in Fig. 1 represent Green's functions with self-energy corrections due to impurity interactions. The first few terms of this contribution to the self-energy are shown in Fig. 5.

B. Tight-binding model, three dimensions

We begin by considering a three-dimensional (3D) sample, and calculate the lowest-order nontrivial correction to the average transmission matrix due to impurity scattering; we thus need to evaluate Figs. 1(a), 1(b), and 5(a). The self-energy is given simply by

$$\Sigma_{3D}^{(i)}=\frac{\mu}{M}\sum_{\mathbf{p}}\frac{1}{\varepsilon-E_0-\varepsilon_p^{\parallel}+\frac{1}{2}i\Gamma_0}\ .$$

Converting the sum to an integral, and noting $L^2/M=a^2$, where L^2 and a^2 are the cross-sectional areas of the well and an impurity, respectively, we find

$$\Sigma_{3D}^{(i)}(\varepsilon)=\mu a^2\int_0^{\Lambda}\frac{dp}{2\pi}p\frac{1}{\varepsilon-E_0-p^2/2m+\frac{1}{2}i\Gamma_0}\ ,$$

where we have set $\varepsilon_p^{\parallel}=p^2/2m$. The quantity $\Lambda\simeq 1/a$ is a cutoff required to keep the integral finite. Performing the integral, we find

$$\mathrm{Re}\Sigma_{3D}^{(i)}(\varepsilon)=\frac{\mu m a^2}{4\pi}\ln\left[\frac{(\varepsilon-E_0-\Lambda^2/2m)^2+(\Gamma_0/2)^2}{(\varepsilon-E_0)^2+(\Gamma_0/2)^2}\right]\ , \tag{3.8a}$$

and

$$\mathrm{Im}\Sigma_{3D}^{(i)}(\varepsilon)=-\frac{\mu m a^2}{2\pi}\Theta(\varepsilon)\ , \tag{3.8b}$$

where

$$\Theta(\varepsilon)=\frac{\pi}{2}+\arctan\left[\frac{2(\varepsilon-E_0)}{\Gamma_0}\right]\ . \tag{3.8c}$$

To find the transmission matrix to lowest order in μ, we need to evaluate Figs. 1(a) and 1(b). We denote these, respectively, as $T^{(0)}(\mathbf{p}_{in},\mathbf{p}_{out};\varepsilon)$ and $T^{(1)}(\mathbf{p}_{in},\mathbf{p}_{out};\varepsilon)$. Using Eqs. (3.8), we find

$$T^{(0)}(\mathbf{p}_{in},\mathbf{p}_{out};\varepsilon)\simeq\frac{\Gamma_0^L\Gamma_0^R}{(\varepsilon-p_{in}^2/2m-E_0)^2+\Gamma_0^2[\frac{1}{2}+\alpha_3\Theta(\varepsilon)]^2}\delta_{\mathbf{p}_{in},\mathbf{p}_{out}}\ , \tag{3.9}$$

where we have noted that $\mathrm{Re}\Sigma_{3D}^{(i)}(\varepsilon)$ is only weakly energy dependent, and have absorbed this into a redefinition of E_0. The quantity α_3 is a unitless measure of the disorder, and is defined as $\alpha_3=\mu m a^2/2\pi\Gamma_0=\rho_{imp}a^4 m V_0^2/2\pi\Gamma_0$. We note that α_3 may be expressed for our short-range impurity-scattering model in terms of the two-dimensional mobility μ^e of the well region; using the lowest-order Born approximation to calculate the collision time, one finds $\alpha_3=e\hbar/2\pi\Gamma_0 m\mu^e$. The imaginary part of the self-energy here introduces an asymmetry in the usual Lorentzian form of the transmission coefficient [Eq. (3.7)]; the low-energy tail now extends out slightly farther than the high-energy tail.

To lowest order in μ, we find for Fig. 1(b)

$$T^{(1)}(\mathbf{p}_{in},\mathbf{p}_{out};\varepsilon)\simeq\frac{\mu}{M}\Gamma_0^L\Gamma_0^R|G_{\mathbf{p}_{in}}^0(\varepsilon)|^2|G_{\mathbf{p}_{out}}^0(\varepsilon)|^2\ , \tag{3.10}$$

where we use the zeroth-order form for the Green's functions because $T^{(1)}$ is explicitly proportional to μ. This contribution has a number of interesting properties. For fixed ε and $\mathbf{p}_{in}$, $T^{(1)}$ depends only on the magnitude of $\mathbf{p}_{out}$, so that the electron "sprays" out into the right reservoir. Furthermore, for $\varepsilon>E_0$, the transmission probability is strongly peaked for states satisfying $\varepsilon-p_{out}^2/2m=E_0$. This defines a cone surface onto which the spraying is favored and hence yields a pronounced spatial distribution in the transmission probability. This focusing effect is actually quite general; one can see from the structure of the diagrams that it persists to all orders in perturbation theory. We will also see below that it occurs in two dimensions, and in a more restricted way in our magnetic field model.

While the spatial distribution of the tunneling current is the most interesting result of this work, it is not the quantity measured in present experiments. Almost all such experiments measure the total current across the DBQW structure.[14] For comparison, we have evaluated the tunneling current for two situations: one for large bias, i.e., a large chemical-potential difference between the reservoirs [Fig. 6(a)], which is the common experimental situation, and one for infinitesimal bias [Fig. 6(b)]. In the former case, if the chemical potential on the right is below the band bottom on the left, the total current at zero temperature may be written approximately as

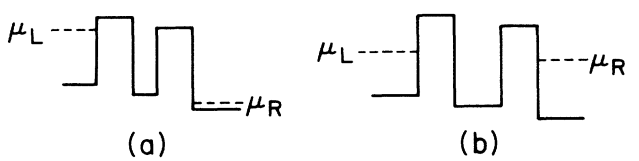

FIG. 6. Chemical potential profile (a) for large-bias case and (b) for infinitesimal bias.

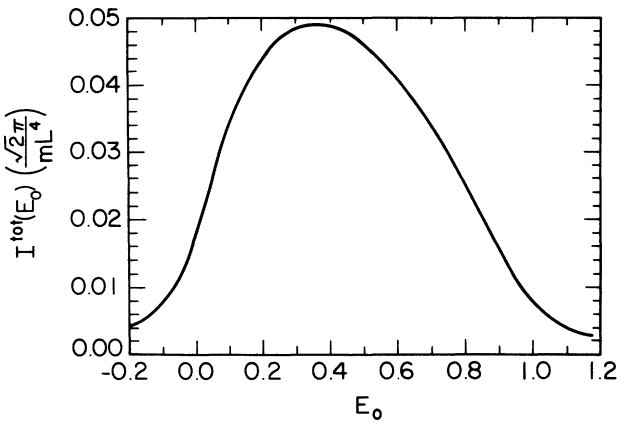

FIG. 7. Total current as a function of E_0 for large bias; $\mu_L=1.0$, $\Gamma_0=0.1$, and $\alpha_3=0.1$.

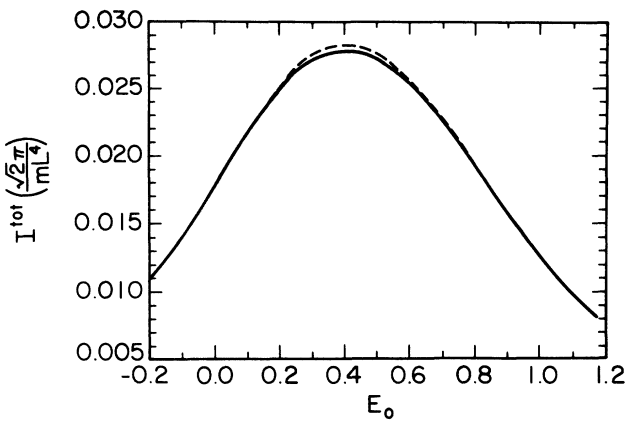

FIG. 8. Total current as a function of E_0 for large bias, with $\mu_L=1.0$ and $\Gamma_0=0.1$. Solid line uses transmission function in Eq. (3.11b), with $\alpha_3=1.0$; dashed line use Breit-Wigner formula [Eq. (3.11c)], with $\Gamma_i=0.6$.

$$I(\mu_L,E_0)\simeq\frac{mL^4}{\sqrt{2}\pi}\Gamma_0^L\Gamma_0^R\int_0^{\mu_L}d\varepsilon\,N(\varepsilon)\times\int_0^{\varepsilon}d\omega\,(\varepsilon-\omega)^{1/2}T^{tot}(\varepsilon,\omega)\,, \tag{3.11a}$$

where

$$T^{tot}(\varepsilon,\omega)=\frac{\Gamma_0^L\Gamma_0^R[1+2\alpha_3\Theta(\varepsilon)]}{(\varepsilon-\omega-E_0)^2+\Gamma_0^2[\frac{1}{2}+\alpha_3\Theta(\varepsilon)]^2}\,, \tag{3.11b}$$

$N(\varepsilon)$ is the density of states, and all energies are measured from the left band bottom. Taking $N(\varepsilon)=N_0$ to be a constant, in Fig. 7 we plot $I(\mu_L,E_0)$ as a function of E_0 for $\Gamma_0=0.1$, $\mu_L=1.0$, and $\alpha_3=0.1$. The asymmetric line shape is typical of these systems and may be understood from basic phase-space considerations.[15,16]

Many past works have resorted to the use of a phenomenological Breit-Wigner form for the transmission coefficient in the presence of incoherent scattering.[4,5] For the purposes of comparison, we have computed the total current for a relatively large impurity density, using both the microscopic equation (3.11b) and the phenomenological Breit-Wigner form

$$T^{tot}_{BW}(\varepsilon,\omega)=\frac{\frac{1}{4}\Gamma_0(\Gamma_0+\Gamma_i)}{(\varepsilon-\omega-E_0)^2+\frac{1}{4}(\Gamma_0+\Gamma_i)^2}\,, \tag{3.11c}$$

where Γ_i is a phenomenological impurity-scattering-induced broadening parameter. In Fig. 8 we plot $I(\mu_L,E_0)$ for both forms of $T^{tot}(\varepsilon,\omega)$, where Γ_i has been chosen such that the currents match at the lowest value of E_0 on the graphs. While the value of α_3 used here is somewhat large for us to work just in the lowest order of perturbation theory, we see that within these approximations the two currents are almost identical.

Clearly, the phase-space factors entering Eq. (3.11a) are much more important than the detailed form of $T^{tot}(\varepsilon,\omega)$ in determining the total current of the DBQW system. This indicates that the Breit-Wigner formula gives a good approximation for the calculation of the total current.

The current for the differential bias case, $\Delta I(E_0,\mu_L)/\Delta\mu$, where $\Delta\mu\equiv\mu_L-\mu_R$, is given to first order in impurity density by

$$\frac{\Delta I(E_0,\mu_L)}{\Delta\mu}=\frac{L^4}{4\pi m}N_0(2m)^{3/2}\int_0^{\mu_L}d\omega\,(\varepsilon-\omega)^{1/2}\frac{1+2\alpha_3\Theta(\varepsilon)}{(\varepsilon-\omega-E_0)^2+\Gamma_0^2[\frac{1}{2}+\alpha_3\Theta(\varepsilon)]^2}\,, \tag{3.12}$$

and is plotted for $\alpha_3=0$, 0.1, and 0.2 in Fig. 9 as a function of μ_L for fixed E_0. We see that the differential current saturates when $\mu_L\simeq\mu_R$ gets well above the resonant energy E_0. As one might intuitively expect, the saturation current decreases with increasing impurity density, and switches over an increasing interval. This latter effect reflects the increased broadening in the transmission line shape as a function of energy due to impurity scattering.

It is interesting to examine the behavior of the perturbation theory at larger values of the impurity density. For such a discussion, it is convenient to express the quantity $\langle|G_{\alpha\beta}(\varepsilon)|^2\rangle$ in the form $|G_\alpha(\varepsilon)|^2\delta_{\alpha\beta}+|G_\alpha(\varepsilon)|^2|G_\beta(\varepsilon)|^2U_{\alpha\beta}(\varepsilon)$, where $\alpha=\mathbf{p}_{in}$ and $\beta=\mathbf{p}_{out}$. So long as the vertex function $U_{\alpha\beta}(\varepsilon)$ is not too strongly dependent upon the final state β, it is clear that the focusing effect will survive at even moderate impurity densities. However, $U_{\alpha\beta}(\varepsilon)$ is not well-behaved for arbitrarily large impurity density. To see this, one can estimate it using the ladder approximation. The result is

$$U_{\alpha\beta}(\varepsilon)\simeq\frac{\mu}{M}\frac{1}{1-2\alpha_3\Theta(\varepsilon)}\,.$$

Within the ladder approximation, $U_{\alpha\beta}(\varepsilon)$ is independent

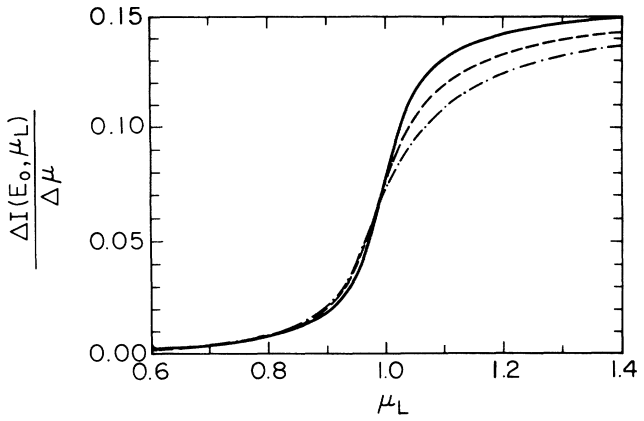

FIG. 9. Differential current as a function of μ_L for $E_0=1.0$, $\Gamma_0=0.1$, and (a) $\alpha_3=0$ (solid line), (b) $\alpha_3=0.1$ (dashed line), and (c) $\alpha_3=0.2$ (dash-dotted line).

of α and β, and thus will not spoil the focusing effect. However, for $\alpha_3>1/2\pi$, $U_{\alpha\beta}(\varepsilon)$ diverges, indicating that the perturbation theory itself breaks down. This is not surprising, because if the impurity scattering is too strong, the resonant tunneling in the system will be spoiled. Indeed, we will see below (Sec. IV) that in the strong-scattering limit the differential conductance has a form very different from that expected for a nearly perfect well: one must interpret the conductance in terms of tunneling through isolated states inside the well rather than a state with a unique resonant energy E_0. Thus, the focusing effect will not survive in the strong-scattering limit; one needs to be in the weak or at least moderate regime $\alpha_3<1/2\pi$. We emphasize, however, that high-quality DBQW structures meet this weak-scattering criterion, as evidenced by the fact that their I-V characteristics can be interpreted as tunneling through a bound state in the well with a unique energy E_0.

C. Tight-binding model, two dimensions

There are a number of reasons for examining the two-dimensional DBQW system. The first, as we shall see below, is that one can evaluate all the second-order corrections to the transmission matrix. More importantly, if an experiment is designed to test the ideas in this work, it will be necessary to probe the current at several locations in the sample. This may be accomplished using microlithographic-nanofabrication techniques on two-dimensional structures. We note that some very recent experiments have already produced structures similar to those that would be needed to test our predictions.[17]

From a calculational point of view, the two-dimensional case is easier to deal with than the three-dimensional case. There turns out to be no necessity to introduce an ultraviolet cutoff in this case, and nearly all the integrals one has to evaluate may be performed using simple contour integration. For example, the self-energy to second order in the impurity density [Figs. 5(a)–5(c)] is given by

$$\Sigma^{(i)}_{2D}(p,\varepsilon)=-i\mu a\sqrt{m/\varepsilon_0}-m(\mu a)^2\frac{1}{\varepsilon_0^2}\left[\frac{2\varepsilon_p^{\parallel}-15\varepsilon_0}{2\varepsilon_p^{\parallel}-9\varepsilon_0}\right], \tag{3.13}$$

where $\varepsilon_0=2(\varepsilon-E_0)+i\Gamma_0$, and the branch cut is chosen such that $\sqrt{\varepsilon_0}$ has a positive imaginary part. We see that the self-energy picks up some momentum dependence at second order in μ; however, for low impurity densities, this has no pronounced effect.

The zeroth-order contribution to the transmission matrix [Fig. 1(a)] is given by

$$T^{(0)}(p_{\rm in},p_{\rm out};\varepsilon)=\Gamma_0^L\Gamma_0^R|G_{p_{\rm in}}(\varepsilon)|^2\delta_{p_{\rm in},p_{\rm out}}$$

with

$$G_{p_{\rm in}}(\varepsilon)\equiv[\varepsilon-E_0-\varepsilon^{\parallel}_{p_{\rm in}}+\Sigma^{(i)}_{2D}(p_{\rm in},\varepsilon)+i\Gamma_0/2]^{-1}\,. \tag{3.14}$$

The result is similar to the three-dimensional case, in that for fixed $p_{\rm in}$, $T^{(0)}$ as a function of ε is essentially Lorentzian, with a weak asymmetry imposed by the energy dependence in $\Sigma^{(i)}_{2D}(p,\varepsilon)$. Since $T^{(0)}$ conserves transverse momentum, this contribution is relatively uninteresting. The next-order contribution to the average transmission matrix, $T^{(1)}(p_{\rm in},p_{\rm out};\varepsilon)$, has the same form as its three-dimensional counterpart [Eq. (3.10)], except one must replace the factors $G^0_{\rm p}(\varepsilon)$ with $G_p(\varepsilon)$ in Eq. (3.14). In Fig. 2, we plotted $T^{(1)}$ as a function of the exit angle (defined in the inset) for $p_{\rm in}=0$ and (a) $\varepsilon<E_0$, and (b) $\varepsilon>E_0$. For $\varepsilon<E_0$, the tunneling electron sprays out into an angular distribution with a width of approximately 1 rad. For $\varepsilon>E_0$, the distribution breaks up into two sharp peaks, centered at angles $\pm\theta_0$ satisfying $\varepsilon-p^2_{\rm out}/2m=\varepsilon\cos^2\theta_0=E_0$. This striking double peaking is the analog of spraying onto a cone surface expected in three dimensions. We note that if the incident electron has a nonzero $p_{\rm in}$, only the overall amplitude of $T^{(1)}$ is affected; the distribution remains symmetric around $\theta=0$.

To see how higher-order terms affect the spatial distribution, we have evaluated Figs. 1(c)–1(f). The sum of these contributions is explicitly proportional to α_2^2, where $\alpha_2=\sqrt{m}\,V_0^2\rho_{\rm imp}a^2/\Gamma_0^{3/2}$, and we denote it as $T^{(2)}(p_{\rm in},p_{\rm out};\varepsilon)$. After a few contour integrals, one finds

$$T^{(2)}(p_{\rm in},p_{\rm out};\varepsilon)=\alpha_2^2\frac{\Gamma_0^{3/2}}{\sqrt{m}\,L}\Gamma_0^R\Gamma_0^L|G^0_{p_{\rm in}}(\varepsilon)|^2\,|G^0_{p_{\rm out}}(\varepsilon)|^2[L(\varepsilon)+J(p_{\rm in}+p_{\rm out},\varepsilon)+2\,{\rm Re}K(p_{\rm in}-p_{\rm out},\varepsilon)]\,,$$

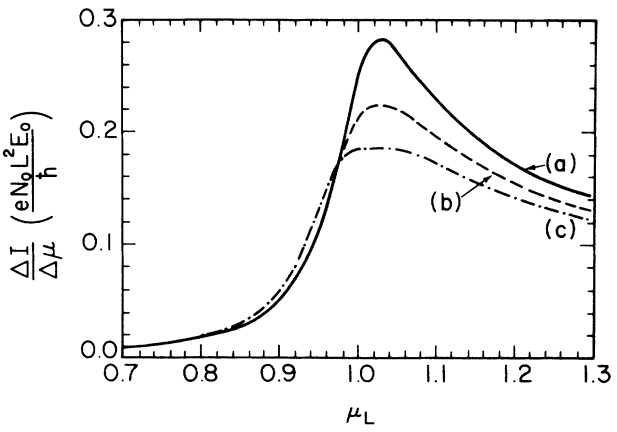

FIG. 10. Differential current for a two-dimensional system as a function of μ_L for $E_0=1.0$, $\Gamma_0=0.1$, and (a) $\alpha_2=0$, (b) $\alpha_2=0.1$, and (c) $\alpha_2=0.2$. N_0 and L are the density of states and size of reservoir, respectively.

where

$$L(\varepsilon)=\Gamma_0^{3/2}|\varepsilon_0|\mathrm{Im}\sqrt{\varepsilon_0}\ ,$$

$$J(p,\varepsilon)=4\Gamma_0^{3/2}\left|\frac{1}{\varepsilon_0}\right|\frac{\mathrm{Im}\sqrt{\varepsilon_0}}{4(\mathrm{Im}\sqrt{\varepsilon_0})^2+2\varepsilon_p^{\parallel}}\ ,$$

$$K(p,\varepsilon)=4i\Gamma_0^{3/2}\frac{1}{\sqrt{\varepsilon_0}}\frac{1}{2\varepsilon_p^{\parallel}-4\varepsilon_0}\ ,$$

are the contributions from Fig. 1(c) (ladder diagram), Fig. 1(d) (crossed diagram), and Figs. 1(e) and 1(f), respectively. In Fig. 3, we plot $T^{(2)}$ as a function of θ for fixed ε and $\varepsilon_{p_{\rm in}}^{\parallel}$. The incident electron is taken to arrive from the second quadrant in the inset of Fig. 2. The spatial distribution of $T^{(2)}$ has the same basic structure as $T^{(1)}$, except that the double peak becomes asymmetric, with a larger "backscattering" than "forward-scattering" peak. In this context, forward scattering and backscattering refer only to the relative directions of $p_{\rm in}$ and $p_{\rm out}$. This contrasts with the behavior well known from weak-localization theory,[18] for which one expects a peak in the scattering at $p_{\rm in}=-p_{\rm out}$. It is interesting to note that the crossed diagram (which is responsible for enhanced backscattering in weak localization) in our calculation does indeed have a maximum at $p_{\rm in}=-p_{\rm out}$. However, this peak is quite broad compared to the Lorentzians multiplying it, and so only shows up in this context as an enhanced weight for the $\theta_0>0$ peak.

We have also evaluated the differential current $\Delta I/\Delta\mu$ as a function of the chemical potential in the reservoirs, μ_L, including terms up to order α_2. The results are presented in Fig. 10. Unlike its three-dimensional counterpart, $\Delta I/\Delta\mu$ for this case does not saturate at large μ_L; one can in fact show that $\Delta I/\Delta\mu\propto 1/\sqrt{\mu_L}$ in the tail region. We see that the main effect of a small impurity density is to lower the peak height and shift the leading edge of the resonance peak slightly back. We will see in Sec. IV that these results agree qualitatively with exact numerical calculations for a finite two-dimensional system.

D. Three dimensions, perpendicular magnetic field

As a final case of interest, we examine the transmission matrix for a three-dimensional sample with a magnetic field perpendicular to the well region. In this situation, if one uses Landau gauge, the relevant transverse quantum numbers are the Landau-level index n and a wave number p. The self-energy to first order in the impurity density is approximately

$$\Sigma_{(\omega)}^{(i)}\simeq\frac{\alpha_m\Gamma^2}{2\pi\omega_c}[\Psi(\tfrac{1}{2}+(E_0-i\Gamma/2-\omega)/\omega_c)-\ln N_c]\ ,$$

where $\omega_c=eB/mc$, B is the magnetic field, $\alpha_m=a^4V_0^2m\omega_c\rho_{\rm imp}/\Gamma_0^2$ is a dimensionless measure of the disorder strength, and Ψ is the digamma function. Note that α_m is explicitly proportional to B. We have introduced a cutoff N_c in the Landau-level summation to keep $\Sigma(\omega)$ finite; for $a\ll l_0$, this is given approximately by $N_c=l_0^2/2a^2$, where $l_0=(\hbar c/eB)^{1/2}$ is the magnetic length. As in the absence of a magnetic field, the divergence in $\Sigma^{(i)}(\omega)$ as $N_c\to\infty$ is an artifact of using the δ-function scatterers. Within the hard-cutoff approximation, we note that

$$\mathrm{Re}\Sigma^{(i)}\simeq\frac{\alpha_m\Gamma_0^2}{2\pi\omega_c}\ln(2a^2eB/c)\ ,$$

which shifts the peak in $T^{(0)}$ slightly upward, by an amount that varies logarithmically with field. To estimate the effect that impurities have on the width of $T^{(0)}$, we evaluate $\mathrm{Im}\Sigma(\omega)$ at $\omega=E_0+\frac{1}{2}\omega_c$ (the resonance associated with tunneling in the lowest Landau level). The result is $\mathrm{Im}\Sigma^{(i)}(\omega)\simeq-i\Gamma_0(\alpha_m/2\pi)$ for $\omega_c\gg\Gamma_0$; the resonance width increases slightly by an amount proportional to B.

To first order in α_m, the self-energy only enters as a correction to the Green's functions in Fig. 1(a). This diagram conserves the Landau index and the wave number p in the tunneling process. The lowest-order contribution to the transmission matrix that allows a nontrivial distribution of final states is given by Fig. 1(b). The average over impurity positions in this case is considerably more difficult to carry out than in the absence of a magnetic field, so we restrict ourselves to the case where the incident electron lies in the lowest Landau level ($n_\alpha=0$). To first order in α_m,

$$T^{(1)}(n_\alpha=0,p_\alpha;n_\beta,p_\beta;\varepsilon)=\Gamma_0^L\Gamma_0^R|G_0^0(\varepsilon)|^2|G_{n_\beta}^0(\varepsilon)|^2\sqrt{2/\pi}\frac{l_0}{L}\alpha_m\Gamma_0^2\exp[-(p_\alpha-p_\beta)^2l_0^2/2]W(n_\beta,-p_\alpha-p_\beta)\ ,$$

where p_α is the incident wave number of the electron, n_β the Landau index of the transmitted electron, and p_β the transmitted wave number. The weighting function $W(n,p)$ is

$$W(n,p)=\frac{1}{2_n\, n!}\sum_{k=0}^{n} 2^k k!\binom{n}{k}^2(-1)^{n-k}H_{2n-2k}(pl_0/i)\ ,$$

where H_n is the nth Hermite polynomial. Note that the transmission matrix is only significant for $|p_\alpha-p_\beta|\sim l_0^{-1}$. This is reasonable, because the electron wave functions are Gaussians of width l_0 centered at pl_0^2; one must expect a tunneling electron with incident wave number p_α to emerge within a distance l_0 of $p_\alpha l_0^2$.

Because p is approximately conserved in the tunneling process, it is useful to sum $T^{(1)}$ over p_β. This leads to the much simpler expression

$$\sum_{p_\beta} T^{(1)}(\alpha,\beta;\varepsilon)=\frac{\alpha_m}{2\pi}\Gamma_0^L\Gamma_0^R\Gamma_0^2|G^0_{n_\alpha}(\varepsilon)|^2\,|G^0_{n_\beta}(\varepsilon)|^2\ .$$

This is formally similar to $T^{(1)}$ for the tight-binding model [Eq. (3.10)], with the transverse momenta replaced by Landau indices. For fixed n_α and ε, this contribution to the transmission matrix is maximized when $\varepsilon-(n_\beta+\frac{1}{2})\omega_c$ is as close as possible to E_0. This is the analog of the focusing effect that led to such striking spatial distributions of the tunneling electron in the absence of a magnetic field.

To illustrate the behavior of $T^{(1)}$, we plot the quantity

$$T^{(1)}_{\rm tot}(n_{\rm in},p_{\rm in};\varepsilon)\equiv\sum_{n_{\rm out}}\sum_{p_{\rm out}} T^{(1)}(n_{\rm in},p_{\rm in};n_{\rm out},p_{\rm out};\varepsilon)$$

in Fig. 11 for $n_{\rm in}=0$, $\Gamma_0=0.1$, $\omega_c=0.1$, and $E_0=1.0$ (which sets the energy scale), as a function of ε. One finds a very large peak at $\varepsilon=E_0+\frac{1}{2}\omega_c$, with weaker peaks superimposed at $\varepsilon=E_0+(n+\frac{1}{2})\omega_c$. These weaker peaks are a direct result of the focusing effect in a magnetic field: whenever the incident energy ε of the electron matches $E_0+(n+\frac{1}{2})\omega_c$, there is an enhanced probability of scattering into the nth Landau level. This is only possible in the presence of scattering; for a pure system, the Landau index must be conserved in the tunneling process.

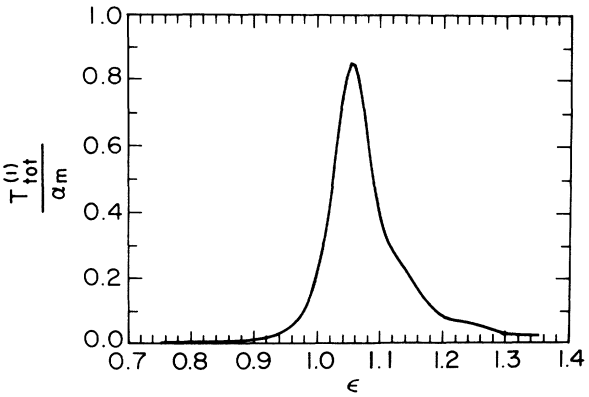

FIG. 11. $T^{(1)}_{\rm tot}$ as a function of ε for $p_{\rm in}=0$, $\omega_c=0.1$, $\Gamma_0=0.1$, and $E_0=1.0$.

IV. NUMERICAL SIMULATION

To check the validity of the perturbation-theory analysis, we have computed the transmission matrix for several two-dimensional finite-size systems, with periodic boundary conditions in one direction, using the recursive Green's-function method.[19] The model used here is the same as our two-dimensional tight-binding model: there is a single row of sites whose average on-site energy may be different than the other on-site energies, and we take the hopping matrix elements connecting this row to the left and right sides of the sample to be smaller than the other hopping matrix elements. We then model the disorder by adding a small, random on-site energy within the well-region row.

In Fig. 12, we show a typical average transmission matrix for fixed incident energy and $p_{\rm in}$ as a function of $p_{\rm out}$. In this particular example, we have examined a system that is 96 sites wide, and have averaged over 32 realizations of the random potential. There is a very sharp peak at $p_{\rm out}=p_{\rm in}$, which corresponds to the $T^{(0)}$ term in our perturbation theory. At a much smaller amplitude, one finds two peaks centered symmetrically around $\theta=0$. This double-peak structure is exactly of the form predicted by the perturbation-theory analysis of Sec. III. We note, furthermore, that the left peak apparently has a slightly larger weight than the right peak, in agreement with our second-order results, $T^{(2)}$.

Superimposed on the broad peak structure is a randomly varying fine structure. This must be expected for any average over a finite number of systems, since the exact transmission differs for different impurity realizations. In Fig. 13, we plot an example of the transmission matrix for a single impurity realization of the same system parameters in Fig. 12. One can see that the fluctuations are quite strong, of the same order of magnitude as the peak heights in the transmission matrix. The focusing effect for a single impurity realization arises as an envelope

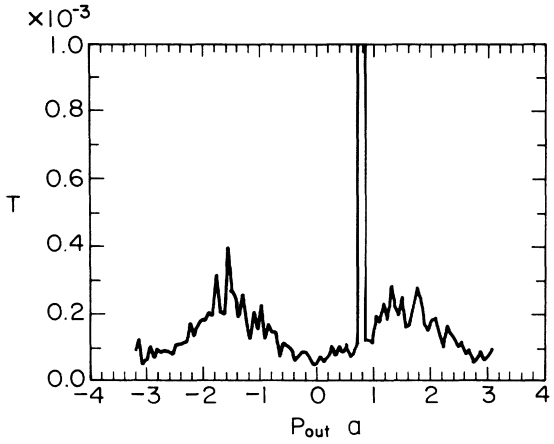

FIG. 12. Transmission matrix as a function of $p_{\rm out}$ for a two-dimensional system 96 sites wide, averaged over 32 impurity realizations. The sharp peak at $p_{\rm out}=p_{\rm in}\simeq 0.9/a$, where a is the separation between sites, corresponds to $T^{(0)}$ in the perturbative analysis, and is far off scale in this plot. The double-peak structure qualitatively agrees with the perturbation-theory analysis.

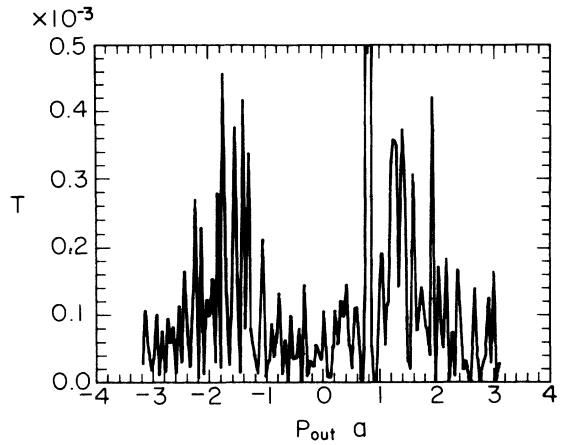

FIG. 13. Transmission matrix for a single impurity realization, with the same system parameters as in Fig. 12. The fluctuations are contained within an envelope function that has the double-peak structure expected for the average transmission matrix.

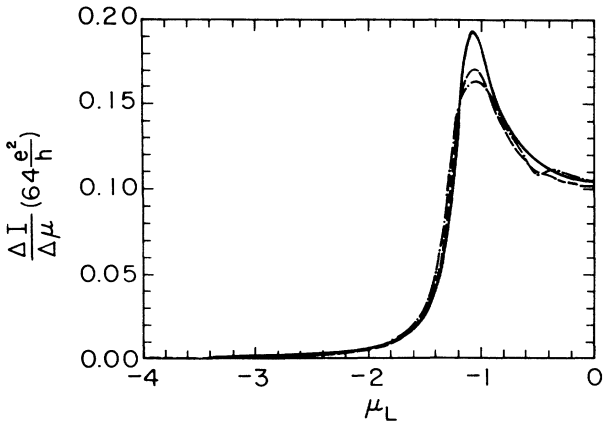

FIG. 14. Differential current as a function of μ_L for a system 64 sites wide, with disorder strengths characterized by (a) $W=0$ (solid line), (b) $W=0.2$ (dashed line), and (c) $W=0.3$ (dash-dotted line).

function for the strongly fluctuating transmission matrix. It is interesting to note that enhanced backscattering effects, which give the left peak a slightly enhanced weight in Fig. 12, manifest themselves as a higher density of fine-structure peaks for negative p_{out} than for positive p_{out}. The peak heights, on the other hand, do not appear systematically larger on either side of the graph.

It is interesting to speculate on whether one expects to observe Fig. 12 or Fig. 13 in a real experimental situation. An experiment is complicated by the fact that one needs a source that can send electrons to the DBQW structure with a well-defined p_{in}. Assuming one can fabricate such a device, it is clear that at the lowest temperatures, one would expect transmitting electrons to have a distribution of p_{out} similar to that in Fig. 13. At higher temperatures, we might expect phase-breaking processes within the well to have an effect similar to averaging over many systems. However, it is an open question whether one in principle can detect the distribution of electron momenta after they have undergone phase-breaking events inside the well, but before they undergo such events outside the well. (Phase-breaking events outside the well would spoil the distribution of momenta intrinsic to the transmission matrix.) We emphasize, however, that even if the experiment is performed in a regime for which the averaging procedure is not appropriate, the focusing effect still will be seen as an envelope function for the fluctuating transmission matrix. Furthermore, since wires collecting the current must have a finite width, and the transmission peaks are quite close together, the current collectors themselves will tend to average out the fine structure.

We have also evaluated numerically the exact differential current $\Delta I/\Delta\mu$ for the two-dimensional finite system. A typical series of graphs for this quantity as a function of the chemical potential μ_L is shown in Fig. 14 for three different disorder strengths. The random potential is generated by adding an on-site potential $\delta\varepsilon_n$ to each site inside the well, where $\delta\varepsilon_n$ is chosen from a flat random distribution between $\pm W/2$. Thus, the disorder strength for the numerical results is characterized by the energy W. One can easily show that the expansion parameter α_2 for the perturbation-theory analysis is proportional to W^2. Figure 14 presents $\Delta I/\Delta\mu$ for $W=0.0$, 0.1, and 0.2, where the energy scale is set by the hopping matrix elements in the reservoir region. We see that the qualitative features of these graphs are quite similar to those of the analytic, perturbative calculation (Fig. 9). As in that case, the peak height is reduced and the leading edge shifts back with increasing disorder. We note that the high-energy tail flattens out for $W=0$ at $\mu_L=0$; this is a finite-size effect, and must be expected due to particle-hole symmetry when the on-site energies in the well and reservoir region are chosen to be the same. There is also some structure in the high-energy tail for the case $W=0.2$; it is likely that this will not remain when one averages over several impurity configurations.

It is also interesting to investigate the differential current in the presence of stronger scattering potentials. In Fig. 15, we present this for an impurity configuration with $W=1.6$ for two values of the hopping matrix elements t^L and t^R, which we take to be identical for this example. For small values of t^L, corresponding to high barriers separating the well region from the reservoirs, we find a series of sharp peaks at different values of the chemical potential μ_L. By evaluating the energy spectrum of an electron in the *isolated* well, one finds that each peak corresponds to a single electron state in the disordered well region. Thus, for each state in the well, there is an essentially Lorentzian resonance peak, whose width Γ_0 is proportional to $(t^L)^2$. As we increase t^L [Fig. 15(b)], the widths increase, so that resonance peaks that are close together merge into broader, smoother structures. The peaks in this figure may then be understood as maxima in the density of states inside the well. It is interesting to note that with barrier heights adjusted to be as large as possible, one can (in principle) directly probe

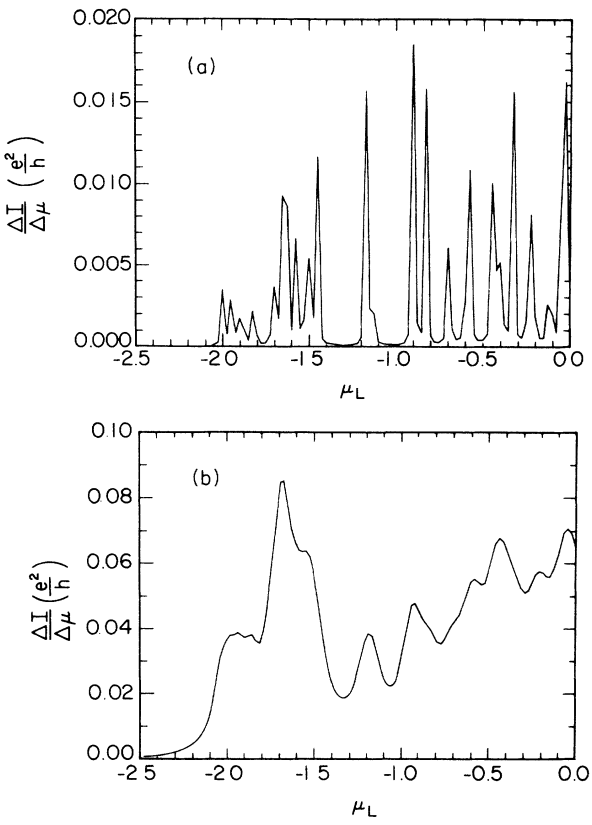

FIG. 15. Differential current $\Delta I/\Delta\mu$ as a function of chemical potential μ_L for $W=1.6$ and well-reservoir coupling matrix elements: (a) $t^R=t^L=0.05$ and (b) $t^R=t^L=0.2$.

the microscopic energy spectrum inside the well region by measuring the conductance of the system. We note that in a very interesting experiment, Kopley and coworkers[20] studied the conductance of a *single*-barrier tunneling structure, for which they found isolated Lorentzian resonances as a function of the gate voltage (which fixed the chemical potential in the reservoirs). They associate these resonances with tunneling through localized electronic states in the barrier; this interpretation seems quite natural in light of our calculations. Unfortunately, there is no direct control over the coupling of these electronic states to the reservoirs in this experiment. Our calculations suggest that the development of devices for which such parameters could be varied independently—for example, by gate structures such as those used in Ref. 17— would lead to the observation of a rich variety of physical phenomena.

V. SUMMARY

We have investigated the effect of elastic scattering in a resonant-tunneling DBQW system. We find that in the absence of a magnetic field, the average transmission matrix shows a striking spatial distribution in the tunneling probability that may be described as a focusing effect. We have verified this result by numerically solving for the transmission matrix of a finite two-dimensional system; there is good qualitative agreement, although there are fluctuations present in the exact solution that only smooth out if one averages over many impurity configurations.

In the presence of a magnetic field, we find that there is a self-energy correction to the usual Lorentzian behavior in the transmission matrix that leads to a slight broadening of the Lorentzian, as well as an upward shift in the resonant energy that varies logarithmically with magnetic field. There is also a contribution to the average transmission matrix from processes that do not conserve Landau-level index; we find that this contribution is maximized when $\varepsilon-(n_\beta+\frac{1}{2})\omega_c$ is as close as possible to the resonant energy E_0, where n_β is the final-state Landau index.

ACKNOWLEDGMENTS

The authors would like to thank Dr. Sungkit Yip for useful conversations. This work was supported by the U.S. Army Research Office (U.S. ARO), the U.S. Office of Naval Research (ONR), and the National Science Foundation (NSF). Computer time was provided by the University of Maryland.

[1]R. W. Keyes, Rev. Mod. Phys. **61**, 279 (1989).
[2]See, for example, E. E. Mendez, J. Phys. (Paris) Colloq. **48**, C5-425 (1987), and references therein.
[3]B. Ricco and M. Ya. Azbel, Phys. Rev. B **29**, 1970 (1984).
[4]B. Gu *et al.*, J. Appl. Phys. **65**, 3510 (1989); R. Gupta and B. K. Ridley, Superlatt. Microstruct. **5**, 417 (1989); T. Weil and B. Vinter, Appl. Phys. Lett. **50**, 1281 (1987); D. D. Coon and H. C. Liu, *ibid.* **49**, 94 (1986); A. D. Stone and P. A. Lee, Phys. Rev. Lett. **54**, 1196 (1985).
[5]M. Büttiker, IBM J. Res. Dev. **32**, 63 (1988).
[6]N. Wingreen, K. W. Jacobsen, and J. W. Wilkins, Phys. Rev. Lett. **61**, 1396 (1988).
[7]M. Jonson, Phys. Rev. B **39**, 5924 (1989).
[8]T. K. Ng and P. A. Lee, Phys. Rev. Lett. **61**, 1768 (1988).
[9]H.A.Fertig and S. Das Sarma, Phys. Rev. B **40**, 7410 (1989).
[10]See, for example, S. Doniach and E. H. Sondheimer, *Green's Functions for Solid State Physicists* (Benjamin, Reading, MA, 1974), p. 98.
[11]C. O. Ambladh and P. Minnhagen, Phys. Rev. B **17**, 929 (1978); G. D. Mahan, *Many Particle Physics* (Plenum, New York, 1981); D. Langreth, Phys. Rev. B **1**, 471 (1970).
[12]E. Merzbahcer, *Quantum Mechanics* (Wiley, New York, 1970).
[13]D. Langreth, Phys. Rev. **150**, 516 (1966).
[14]See, for example, V. J. Goldman, D. C. Tsui, and J.E. Cunningham, Phys. Rev. Lett. **58**, 1268 (1987).
[15]S. Luryi, Appl. Phys. Lett. **47**, 490 (1985).
[16]H. C. Liu and G. C. Aers, Solid State Commun. **67**, 1131 (1988).
[17]A. Palevski *et al.*, Phys. Rev. Lett. **62**, 1776 (1989).
[18]P. A. Lee and T. V. Ramakrishnan, Rev. Mod. Phys. **57**, 287 (1985).
[19]P. A. Lee and D. S. Fisher, Phys. Rev. Lett. **47**, 882 (1981).
[20]T. E. Kopley, P. L. McEven, and R. G. Wheeler, Phys. Rev. Lett. **61**, 1654 (1988).